Int. J. Electrochem. Sci., 10 **(2015)** 8412 - 8422

International Journal of
ELECTROCHEMICAL
SCIENCE
www.electrochemsci.org

Electrochemical Evaluation of $La_{1-x}Ca_xMnO_3$ in Zinc-air Batteries

Guanghua Li, Mohammed Adnan Mezaal, Rui Zhang, Ke Zhang, Wei Liu, Lixu Lei[*]

School of Chemistry and Chemical Engineering, Southeast University, Nanjing 211189, China
[*]E-mail: lixu.lei@seu.edu.cn

Received: 9 July 2015 / *Accepted:* 31 July 2015 / *Published:* 26 August 2015

In this article, $La_{1-x}Ca_xMnO_3$ (x = 0.1 ~ 0.4) of perovskite type as bi-functional catalysts for primary and rechargeable zinc-air battery has been prepared with their structure and morphology examined by means of XRD and SEM. Based on the polarization curves, the catalysts exhibit similar catalytic activities for both oxygen evolution reaction and oxygen reduction reaction, but $La_{0.8}Ca_{0.2}MnO_3$ shows the best battery performance because of its high specific capacity, lowest discharge-charge voltage gap, and lowest degradation during cycles.

Keywords: ZABs; OER; ORR; Perovskites, Gas-diffusion electrode

1. INTRODUCTION

With attention to the consciousness of environmental protection and renewable, people are paying more attention to the metal-air batteries [1]. Compared with the traditional battery such as lithium ion batteries, nickel cadmium batteries, and lead-acid batteries, metal-air batteries possess good security and high theoretical energy density [2]. Recently, many metal-air batteries for example, silicon-air batteries [3], sodium-air batteries [4], germanium-air batteries [5], aluminum-air batteries [6], tungsten-air batteries [7], iron-air batteries [8], titanium-air batteries [9], lithium-air batteries [10], and zinc-air batteries (ZABs) [11] have been reported. Among metal-air batteries, ZABs have attracted much attention because of their high energy conversion efficiency and low emission.

Gas diffusion electrodes (GDEs) are one of the most roles of ZABs. Typical GDEs are consist of a gas diffusion layer, a current collector [12, 13], and a catalyst layer (CL) [14, 15]. The gas diffusion layer (GDL) is consist of carbon materials and binder (60 wt% PTFE suspensions) and act preventing electrolyte permeation with O_2 diffuses into the CL. The CL is made from conductive carbon, catalyst, and binder. The oxygen reduction and oxygen evolution mainly occur in the catalyst

layer [16]. For ORR in alkaline condition, atmospheric O_2 diffuses into the CL from the GDL, where it is reduced to OH^- at the three-phase boundary between O_2, KOH aqueous solution and air electrode [17]. The OER process is just the opposite. Thus, the structure of GDEs and the ORR or OER catalytic activity of catalyst are emphasis for improvement performance.

Nowadays, many types of non-noble catalysts for example transition metal oxides in form of perovskites [18-21], spinels [22-24] and their dopant [25, 26] have been reported. Especially, the perovskite oxides were widely studied as GDEs material for ZABs, owing to its high catalytic activity for ORR/OER and excellent stability in alkaline solution [27, 28]. For the A-site replaced by lanthanum of large ionic radius make for oxygen adsorption [29]. For the B-site replaced by transition metal influences the activity of sorbed oxygen [30]. Nanocrystalline perovskite of composition $La_{0.6}Ca_{0.4}CoO_3$ shows excellent electrocatalytic activity for oxygen evolution/oxygen reduction in alkaline solution [31]. The $La_{0.7}Sr_{0.3}Co_{0.7}Fe_{0.3}O_3$ is an excellent catalyst for the rechargeable ZABs [32]. Yuasa et al. [33] synthesized the $LaMnO_3$, $LaMn_{0.6}Fe_{0.4}O_3$, and $La_{0.4}Ca_{0.6}Mn_{0.6}Fe_{0.4}O_3$ perovskite catalysts and demonstrated their durability and ORR activity.

In this work, for A-site Calcium-doped $LaMnO_3$ perovskite oxides (Ca-subsitution, 0.1 ~ 0.4 mol) were prepared by the citrate method. They as electrocatalysts of GDEs have been investigated the catalytic properties towards ORR and OER. And, the gas diffusion layer of GDEs has been replaced by PTFE membrane, which simplified the production process. The performance of the samples was evaluated for primary and rechargeable zinc-air batteries in homemade electrochemical single cell.

2. EXPERIMENTAL

2.1 Synthesis of $La_{1-x}Ca_xMnO_3$ and characterization

Ca doped $LaMnO_3$ perovskite was synthesized by the citrate method [34]. Lanthanum nitrate hexahydrate, calcium nitrate terahydrate, manganese nitrate terahydrate and citric acid were mixed in a stoichiometric molar ratio of $La_{1-x}Ca_xMnO_3$ (x = 0.1 ~ 0.4) and dissolved in ethanol. After that citric acid was added while stirring strongly. The mixture was maintained at 70 °C for 4 h to remove excess solvents, which was dried at 100 °C overnight. The gel precursor was heated at 200 °C until it formed ash. The collected ash was ground and then heated at 700 °C for 2 h in stagnant air furnace to form $La_{1-x}Ca_xMnO_3$ powder.

The perovskite morphology was examined by a scanning electron microscope (SEM), which was attached to an energy dispersive spectrometer (EDS). The structure was carried out with an X-ray diffractometer (XRD). La, Ca and Mn contents of the samples were performed by an inductively coupled plasma-atomic emission spectrometry (ICP). Thermogravimetric (TGA) curves were performed with a thermal analyzer.

2.2 Fabrication of air electrode and ZABs and testing

The air electrode composed of a GDL, a current collector, and a CL. To prepare the CL, a mixture including $La_{1-x}Ca_xMnO_3$ (x = 0.1 ~ 0.4) catalyst and acetylene black (AB) was milled for half

hour, after that the mixture and binder (60 wt% PTFE suspension) at a weight ratio of 8:2 were mingled, milled and dried, respectively, which was rolled into a Ni-screen. Another side was attached a polytetrafluoroethylene membrane as a GDL.

The discharge and polarization curves were carried out using a half-cell with an electrochemical workstation. The cathode, a home-made Hg/HgO electrode, a nickel sheet, and 7 M KOH aqueous solution was used as the working electrode, a reference electrode, a counter electrode, and electrolyte, respectively. A homebuilt zinc-air single cell device was prepared about ZABs testing.

3. RESULTS AND DISCUSSION

3.1 Physical characterization of $La_{1-x}Ca_xMnO_3$

To understand the decomposition behaviors of $La_{1-x}Ca_xMnO_3$ precursor, the TGA curve of $La_{0.8}Ca_{0.2}MnO_3$ precursor are shown in Fig. 1. The curve contains two processes of mass loss. The first process between 50 °C and 180 °C indicates a small mass loss, which attributed to the elimination of free water in sample. The second process between 180 °C and 600 °C shows a large mass loss of 48.38% manifesting that a stable perovskite crystallized completely has formed. After 600 °C, the TGA curve has not step of weight loss and appears a relatively steady state. This result indicates that a stable perovskite crystallized completely has formed. In order to ensure that all the samples can be completely converted to corresponding perovskites, 700 °C was employed.

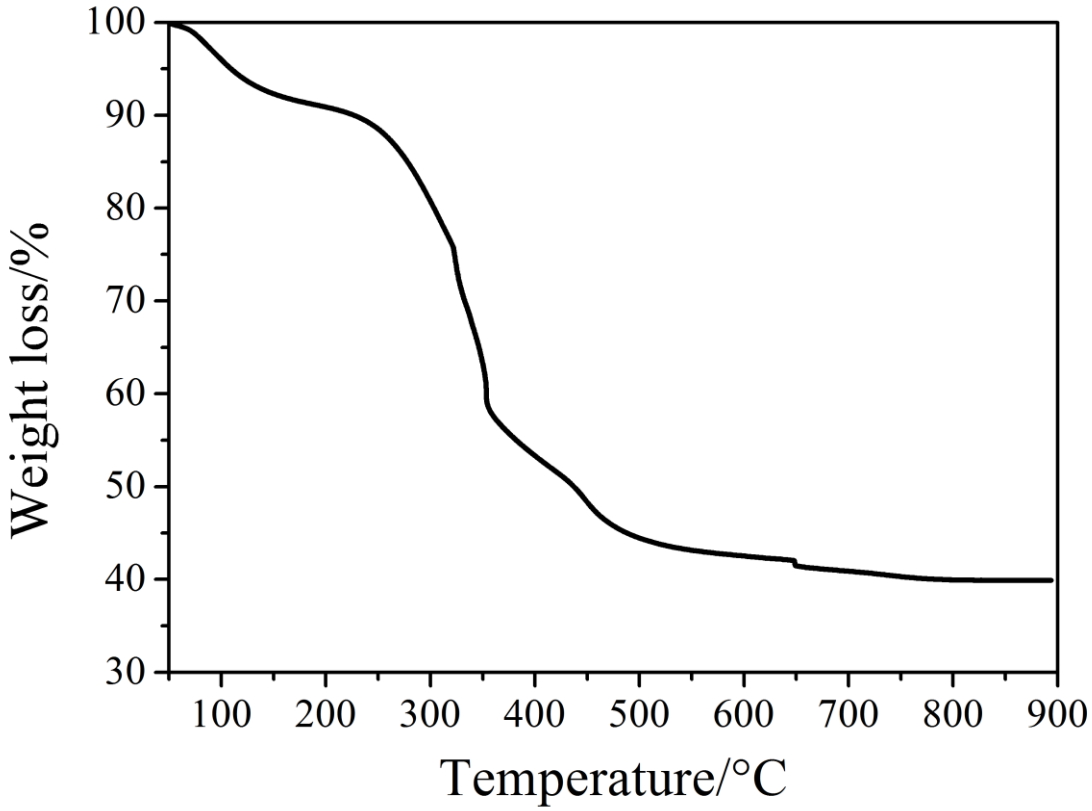

Figure 1. TGA curve of $La_{0.8}Ca_{0.2}MnO_3$ precursor

The XRD patterns for the $La_{0.6}Ca_{0.4}MnO_3$, $La_{0.7}Ca_{0.3}MnO_3$, $La_{0.8}Ca_{0.2}MnO_3$ and $La_{0.9}Ca_{0.1}MnO_3$ are shown in Fig. 2. All the diffraction peaks can be indexed to perovskite-type structure with a primitive cubic cell, P_m-3m (no. 221) space group, which agree well with the reported data (PDF89-5717), and the lattice parameters are recorded in Table 1, which shows that the values $a = b = c$ increase as content of La increases. It is well-known that La^{3+} occupies the 12-coordinated position and Mn^{3+} takes the octahedral position in the perovskite structure, and substitution of La^{3+} for Sr^{2+} requires either Mn^{3+} being oxidized to Mn^{4+} or some of the oxygen atoms absent to maintain the electric neutrality. This certainly changes the size of the lattice cell.

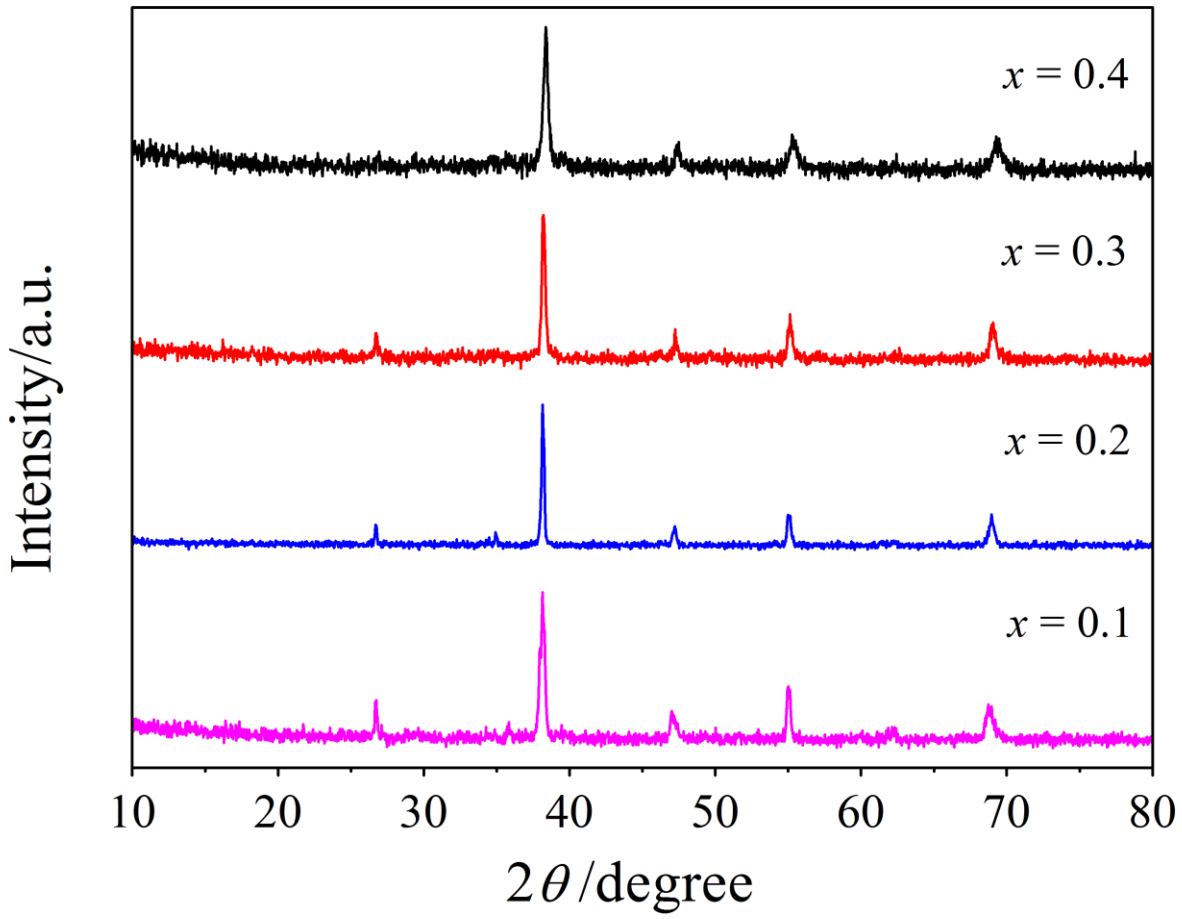

Figure 2. XRD patterns of $La_{1-x}Ca_xMnO_3$

Table 1. The lattice parameters of $La_{1-x}Ca_xMnO_3$

Compose	$La_{0.6}Ca_{0.4}MnO_3$	$La_{0.7}Ca_{0.3}MnO_3$	$La_{0.8}Ca_{0.2}MnO_3$	$La_{0.9}Ca_{0.1}MnO_3$
a (Å)	3.8188	3.8332	3.8378	3.8440

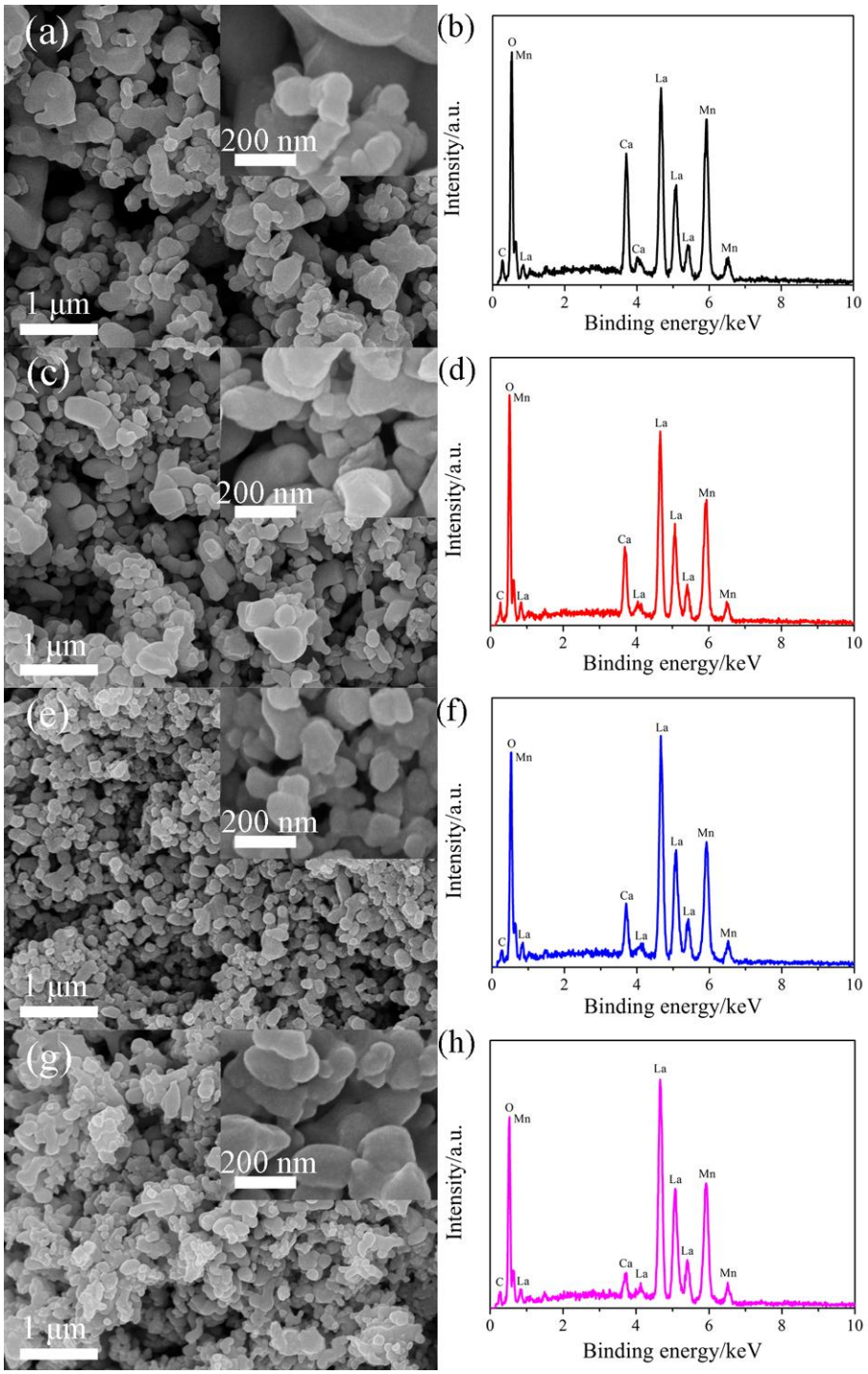

Figure 3. SEM images and EDS spectra of (a, b) $La_{0.6}Ca_{0.4}MnO_3$, (c, d) $La_{0.7}Ca_{0.3}MnO_3$, (e, f) $La_{0.8}Ca_{0.2}MnO_3$ and (g, h) $La_{0.9}Ca_{0.1}MnO_3$, respectively.

Fig. 3 (a, c, e and g) shows the SEM images of $La_{0.6}Ca_{0.4}MnO_3$, $La_{0.7}Ca_{0.3}MnO_3$, $La_{0.8}Ca_{0.2}MnO_3$ and $La_{0.9}Ca_{0.1}MnO_3$, respectively, which illustrate the irregular aggregated particles with an average diameter of 200 ~ 500 nm. It can be seen that the particles of $La_{0.8}Ca_{0.2}MnO_3$ are smaller (100 ~ 200 nm) than $La_{0.6}Ca_{0.4}MnO_3$, $La_{0.7}Ca_{0.3}MnO_3$ and $La_{0.9}Ca_{0.1}MnO_3$. The corresponding EDS spectrum was also shown in Fig. 3 (b, d, f and h), respectively.

La, Ca and Mn contents of the samples were carried out by ICP. Herein, according to the different weight ratios $La_{1-x}Ca_xMnO_3$ (x = 0.1 ~ 0.4). The chemical formula of the materials is $La_{0.62}Ca_{0.38}MnO_3$, $La_{0.73}Ca_{0.27}MnO_3$, $La_{0.80}Ca_{0.20}MnO_3$ and $La_{0.91}Ca_{0.09}MnO_3$, respectively, and is very close to the proposed $La_{0.6}Ca_{0.4}MnO_3$, $La_{0.7}Ca_{0.3}MnO_3$, $La_{0.8}Ca_{0.2}MnO_3$ and $La_{0.9}Ca_{0.1}MnO_3$ chemical stoichiometry, respectively (see Table 1).

Table 2. Element content of the $La_{1-x}Ca_xMnO_3$ (x = 0.1 ~ 0.4).

Compose		La (mg/g)	Ca (mg/g)	Mn (mg/g)
Proposed	Found			
$La_{0.6}Ca_{0.4}MnO_3$	$La_{0.62}Ca_{0.38}MnO_3$	412 (422)	79.2 (74.5)	272 (269)
$La_{0.7}Ca_{0.3}MnO_3$	$La_{0.73}Ca_{0.27}MnO_3$	458 (471)	56.7 (50.3)	259 (255)
$La_{0.8}Ca_{0.2}MnO_3$	$La_{0.80}Ca_{0.20}MnO_3$	500 (500)	36.1 (36.1)	247 (247)
$La_{0.9}Ca_{0.1}MnO_3$	$La_{0.91}Ca_{0.09}MnO_3$	539 (543)	17.3 (15.5)	237 (236)

* Values are found (calculated according to the found compositions)

3.2 Electrocatalytic ORR and OER

The Cathodic and anodic polarization [35] were carried out for the ORR and OER, respectively. The polarization curves of $La_{0.6}Ca_{0.4}MnO_3$, $La_{0.7}Ca_{0.3}MnO_3$, $La_{0.8}Ca_{0.2}MnO_3$ and $La_{0.9}Ca_{0.1}MnO_3$ are shown in Fig. 4. The air electrodes with $La_{1-x}Ca_xMnO_3$ (x = 0.1 ~ 0.4) catalysts were measured as the ORR and OER overpotentials, respectively. On the cathodic branch, the overpotential was 95, 72, 53 and 87 mV, respectively (at 10 mA cm^{-2}). The $La_{0.8}Ca_{0.2}MnO_3$ catalyst operated 42, 19 and 34 mV positive potential than $La_{0.6}Ca_{0.4}MnO_3$, $La_{0.7}Ca_{0.3}MnO_3$ and $La_{0.9}Ca_{0.1}MnO_3$, respectively. The $La_{0.8}Ca_{0.2}MnO_3$ has the optimal property towards to ORR. On the anodic branch, at the same current density (10 mA cm^{-2}), the overpotential was 688, 648, 619 and 706 mV, respectively. The $La_{0.8}Ca_{0.2}MnO_3$ catalyst operated 69, 29 and 87 mV more negative potential than $La_{0.6}Ca_{0.4}MnO_3$, $La_{0.7}Ca_{0.3}MnO_3$ and $La_{0.9}Ca_{0.1}MnO_3$, respectively. Uniformly, $La_{0.8}Ca_{0.2}MnO_3$ has the optimal property towards to OER. The ORR/OER property was estimated by making the difference of potentials between −10 mA cm^{-2} and 10 mA cm^{-2}. The difference of potential of $La_{0.6}Ca_{0.4}MnO_3$, $La_{0.7}Ca_{0.3}MnO_3$, $La_{0.8}Ca_{0.2}MnO_3$, and $La_{0.9}Ca_{0.1}MnO_3$ catalysts is found to be 783, 720, 672 and 793 mV, respectively. For comparison, $La_{0.8}Ca_{0.2}MnO_3$ as excellent bi-functional activity catalyst was observed.

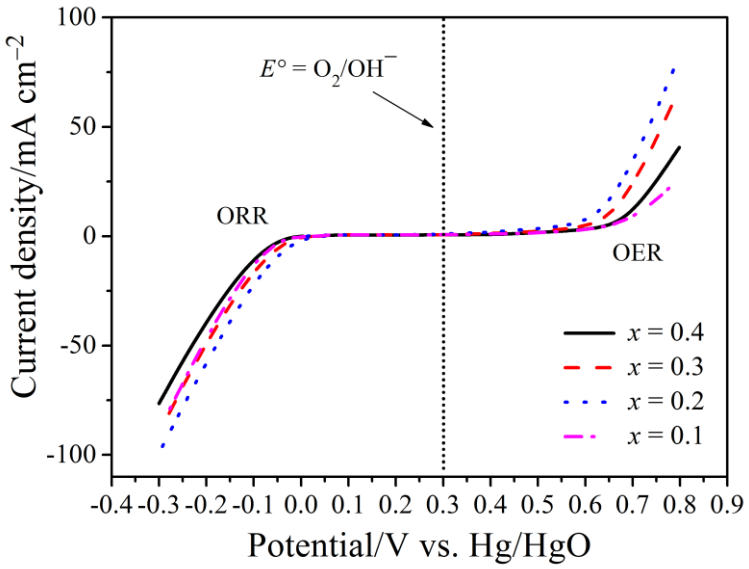

Figure 4. ORR and OER polarization curves of the GDEs with $La_{1-x}Ca_xMnO_3$.

3.3 Primary zinc-air batteries tests

The ORR activity of the $La_{1-x}Ca_xMnO_3$ (x = 0.1 ~ 0.4) perovskite powder is further evaluated in a zinc-air cell. Polarization and power density curves of air electrodes with $La_{0.6}Ca_{0.4}MnO_3$, $La_{0.7}Ca_{0.3}MnO_3$, $La_{0.8}Ca_{0.2}MnO_3$ and $La_{0.9}Ca_{0.1}MnO_3$ catalysts are displayed in Fig. 5. Single cell ORR current density of 44.3, 55.2, 62.2 and 53.0 mA cm^{-2} was obtained at a voltage of 1.0 V, respectively. The peak power density of $La_{0.8}Ca_{0.2}MnO_3$ reached to 98.0 mW cm^{-2} (at 168.5 mA cm^{-2}) in ZABs, which is around 41%, 14% and 17% higher than that of $La_{0.6}Ca_{0.4}MnO_3$ (69.5 mW cm^{-2} at 116.5 mA cm^{-2}), $La_{0.7}Ca_{0.3}MnO_3$ (85.8 mW cm^{-2} at 145.1 mA cm^{-2}) and $La_{0.9}Ca_{0.1}MnO_3$ (84.1 mW cm^{-2} at 144.5 mA cm^{-2}) catalyst, respectively.

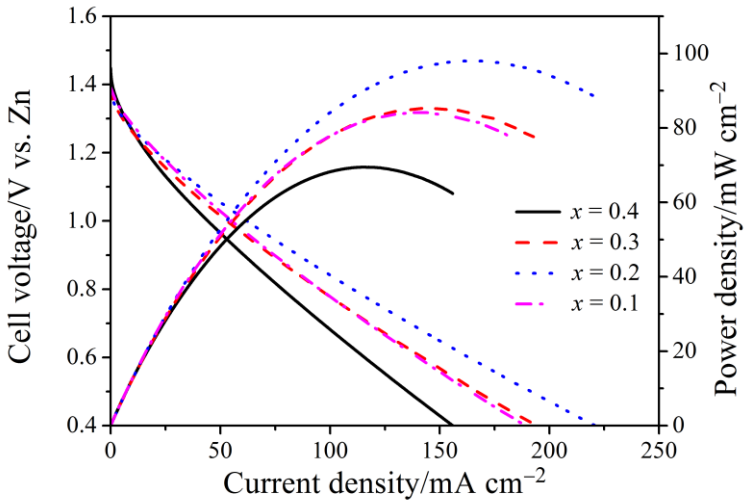

Figure 5. Polarization and power density curves for ZABs with $La_{1-x}Ca_xMnO_3$

To demonstrate the practical application of $La_{1-x}Ca_xMnO_3$ (x = 0.1 ~ 0.4) perovskite, we prepare the air electrode and evaluate its performance in ZABs under realistic conditions. Clearly, as shown in Fig. 6, primary zinc-air batteries made with $La_{0.6}Ca_{0.4}MnO_3$, $La_{0.7}Ca_{0.3}MnO_3$, $La_{0.8}Ca_{0.2}MnO_3$ and $La_{0.9}Ca_{0.1}MnO_3$ were original. The discharge time last for 17.6, 21.4, 23.4 and 21.1 h (at 30 mA cm^{-2} (Fig. 6a)), and for 12.0, 14.8, 15.0 and 12.8 h (at 50 mA cm^{-2} (Fig. 6b)), respectively. It was owing to the stability of $La_{1-x}Ca_xMnO_3$ (x = 0.1 ~ 0.4) towards ORR [36]. The specific capacity normalized to the weight of consumed zinc [37] was 412.1, 501.2, 547.5 and 494.8 at 30 mA cm^{-2}, or was 469.9, 575.5, 584.1 and 501.1 mAh g^{-1} at 50 mA cm^{-2}, respectively. These data suggest that $La_{1-x}Ca_xMnO_3$ (x = 0.1 ~ 0.4) perovskite catalyst can provide better performance in accordance with the polarization and the power density results (Fig. 5). The $La_{0.8}Ca_{0.2}MnO_3$ is optimal for primary ZABs because of the high specific capacity (corresponding to >700 Wh kg^{-1}) and durability [38].

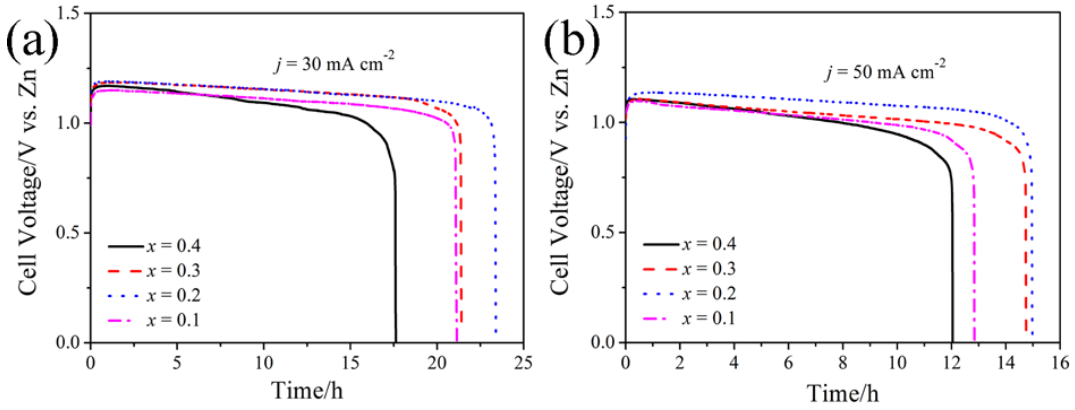

Figure 6. Discharge curves of ZABs with $La_{1-x}Ca_xMnO_3$; a at 30 and b at 50 mA cm^{-2}

3.4 Rechargeable zinc-air batteries tests

Fig. 7 displays the charge/discharge polarization curves of $La_{0.6}Ca_{0.4}MnO_3$, $La_{0.7}Ca_{0.3}MnO_3$, $La_{0.8}Ca_{0.2}MnO_3$ and $La_{0.9}Ca_{0.1}MnO_3$ catalyst loaded on Ni foam for ORR/OER electrodes in rechargeable ZABs. The charge/discharge voltage gap at 10 mA cm^{-2} was 1.23, 1.19, 1.15 and 1.21 V, respectively. Clearly, the voltage gap of the battery with $La_{0.8}Ca_{0.2}MnO_3$ catalyst is much smaller than $La_{0.6}Ca_{0.4}MnO_3$, $La_{0.7}Ca_{0.3}MnO_3$ and $La_{0.9}Ca_{0.1}MnO_3$. This test results suggest that high ORR-OER activity of $La_{0.8}Ca_{0.2}MnO_3$ the actually function as a replaceable bi-functional catalyst for ZABs [39].

Building on the promising half-cell performance, zinc-air battery adopting a zinc electrode was used to evaluate the $La_{1-x}Ca_xMnO_3$ (x = 0.1 ~ 0.4) catalyst´s performance under realistic operating conditions. The stability of the $La_{1-x}Ca_xMnO_3$ (x = 0.1 ~ 0.4) samples were performed by the charge-discharge cycling. The battery was performed by discharging and charging at 10 mA cm^{-2} (600 s in each state). The first ten cycles displays the same discharge potential and a lower charge potential (Fig. 8). The final charge and discharge potential of $La_{0.8}Ca_{0.2}MnO_3$ was almost reached at ~ 2.13 and ~ 1.13 V after 60 cycles, but the original values were ~ 2.38 and ~ 1.22 V. The difference of potentials [40] for initial and discharge process for $La_{0.8}Ca_{0.2}MnO_3$ after 60 cycles was ~ 1.16 V compared to the

initial ~ 1.00 V with a small difference of 0.16 V. The lower voltage gap shown by $La_{0.8}Ca_{0.2}MnO_3$, which indicated better rechargability for rechargeable ZABs [41].

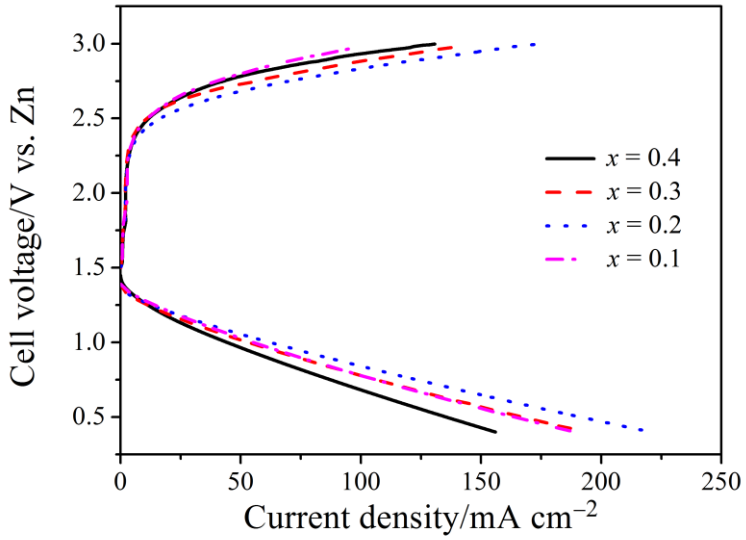

Figure 7. Charge and discharge polarization curves ofthe ZABs with $La_{1-x}Ca_xMnO_3$

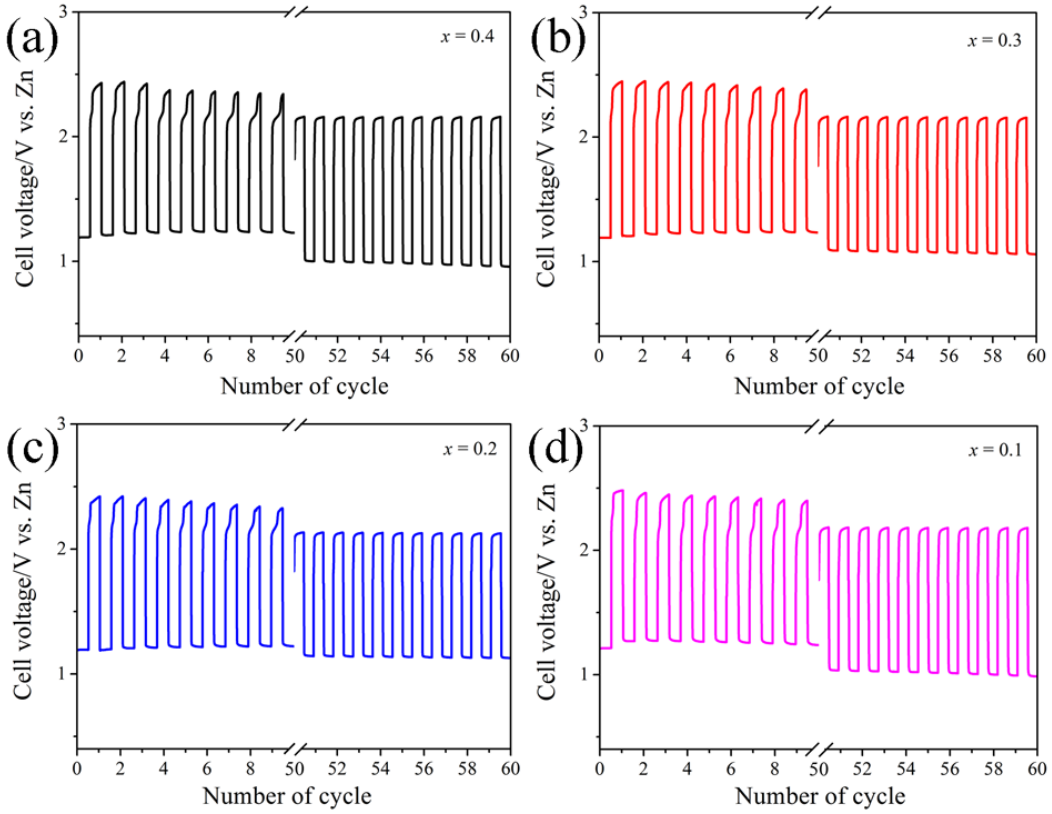

Figure 8. Charge-discharge cycling of the ZABs with $La_{1-x}Ca_xMnO_3$

4. CONCLUSIONS

The $La_{1-x}Ca_xMnO_3$ (x = 0.1 ~ 0.4) powder was prepared at a low cost approach. XRD patterns show that the $La_{1-x}Ca_xMnO_3$ (x = 0.1 ~ 0.4) have perovskite structure. Electrochemical estimation indicated that the $La_{1-x}Ca_xMnO_3$ (x = 0.1 ~ 0.4) are a replaceable catalyst towards to ORR and OER in alkaline condition, especially $La_{0.8}Ca_{0.2}MnO_3$. The highest maximum power density of 98.0 mW cm^{-2} was achieved. The smallest potential difference between charging and discharging was 1.0 V. The battery shows 10-h charge-discharge cycling stability at 10 mA cm^{-2}. In conclusion, the optimum Ca doped $LaMnO_3$ was $La_{0.8}Ca_{0.2}MnO_3$ in primary and rechargeable ZABs in our study.

ACKNOWLEDGMENTS
This work was supported by Analytical Test Fund of Southeast University (201226).

References

1. M. Armand, J.-M. Tarascon, *Nature* 451 (2008) 652-657.
2. F. Cheng, J. Chen, *Chem. Soc. Rev.* 41 (2012) 2172-2192.
3. G. Cohn, R.A. Eichel, Y. Ein-Eli, *Phys. Chem. Chem. Phys.* 15 (2013) 3256-3263.
4. W. Liu, Q. Sun, Y. Yang, J.Y. Xie, Z.W. Fu, *Chem. Commun.* 49 (2013) 1951-1953.
5. J.D. Ocon, J.W. Kim, S. Uhm, B.S. Mun, J. Lee, *Phys. Chem. Chem. Phys.* 15 (2013) 6333-6338.
6. Z. Zhang, C. Zuo, Z. Liu, Y. Yu, Y. Zuo, Y. Song, *J. Power Sources* 251 (2014) 470-475.
7. X. Zhao, X. Li, Y. Gong, N. Xu, K. Romito, K. Huang, *Chem. Commun.* 49 (2013) 5357-5359.
8. X. Zhao, N. Xu, X. Li, Y. Gong, K. Huang, *RSC Adv.* 2 (2012) 10163-10166.
9. Van der Ven, B. Puchala, T. Nagase, *J. Power Sources* 242 (2013) 400-404.
10. Z. Peng, S.A. Freunberger, Y. Chen, P.G. Bruce, *Science* 337 (2012) 563-566.
11. S. Zhu, Z. Chen, B. Li, D. Higgins, H. Wang, H. Li, Z. Chen, *Electrochim. Acta* 56 (2011) 5080-5084.
12. F. Bidault, D.J.L. Brett, P.H. Middleton, N. Abson, N.P. Brandon, *Int. J. Hydrogen Energ.* 34 (2009) 6799-6808.
13. G.M. Huang, M.H. Chang, *Int. J. Electrochem. Sci.* 9 (2014) 7819-7831.
14. Z. Wei, W. Huang, S. Zhang , J. Tan, *J. Power Sources* 91 (2000) 83-85.
15. F. Bidault, D.J.L. Brett, P.H. Middleton, N.P. Brandon, *J. Power Sources* 187 (2009) 39-48.
16. Weidenkaff, S.G. Ebbinghaus, T. Lippert, M.J. Montenegro, C. Soltmann, R. Wessicken, *Cryst. Eng.* 5 (2002) 449-457.
17. M. Yuasa, N. Tachibana, K. Shimanoe, *Chem. Mater.* 25 (2013) 3072-3079.
18. W. Zhou, J. Sunarso, *J. Phys. Chem. Lett.* 4 (2013) 2982-2988.
19. M. Yuasa, H. Imamura, M. Nishida, T. Kida, K. Shimanoe, *Electrochem. Commun.* 24 (2012) 50-52.
20. J. Sunarso, A.A.J. Torriero, W. Zhou, P.C. Howlett, M. Forsyth, *J. Phys. Chem. C* 116 (2012) 5827-5834.
21. S. Zhuang, H. Zhang, S. Liu, F. Tu, W. Zhang, C. Zhao, *Int. J. Electrochem. Sci.* 9 (2014) 1690-1701.
22. X. Ge, Y. Liu, F.W. Goh, T.S. Hor, Y. Zong, P. Xiao, Z. Zhang, S.H. Lim, B. Li, X. Wang, Z. Liu, *ACS Appl. Mater. Inter.* 6 (2014) 12684-12691.
23. M. Prabu, P. Ramakrishnan, S. Shanmugam, *Electrochem. Commun.* 41 (2014) 59-63.
24. M. Prabu, K. Ketpang, S. Shanmugam, *Nanoscale* 6 (2014) 3173-3181.
25. A. Morozan, B. Jousselme, S. Palacin, *Energ. Environ. Sci.* 4 (2011) 1238-1254.

26. Y. Liang, H. Wang, J. Zhou, Y. Li, J. Wang, T. Regier, H. Dai, *J. Am. Chem. Soc.* 134 (2012) 3517-3523.
27. M. Yuasa, M. Nishida, T. Kida, N. Yamazoe, K. Shimanoe, *J. Electrochem. Soc.* 158 (2011) A605-A610.
28. J. Suntivich, H.A. Gasteiger, N. Yabuuchi, H. Nakanishi, J.B. Goodenough, S.H. Yang, *Nat. Chem.* 3 (2011) 546-550.
29. T. Hyodo, M. Kayashi, N. Miura, N. Yamazoe, *J. Electrochem. Soc.* 143 (1996) L266-L267.
30. J. Suntivich, K.J. May, H.A. Gasteiger, J.B. Goodenough, Y. Shao-Horn, *Science* 334 (2011) 1383-1385.
31. S. Malkhandi, B. Yang, A.K. Manohar, A. Manivannan, G.K.S. Prakash, S.R. Narayanan, *J. Phys. Chem. Lett.* 3 (2012) 967-972.
32. S. Ahn, K. Kim, H. Kim, S. Nam, S. Eom, Physica Scripta T139 (2010) *doi:10.1088/0031-8949/2010/T1139/014014.*
33. M. Yuasa, N. Yamazoe, K. Shimanoe, *J. Electrochem. Soc.* 158 (2011) A411.
34. X. Wang, P.J. Sebastian, M.A. Smit, H. Yang, S.A. Gamboa, *J. Power Sources* 124 (2003) 278-284.
35. S.W. Eom, S.Y. Ahn, I.J. Kim, Y.K. Sun, H.S. Kim, *J. Electroceram.* 23 (2008) 382-386.
36. G.Q. Zhang, X.G. Zhang, *Electrochim. Acta* 49 (2004) 873-877.
37. M. Prabu, P. Ramakrishnan, H. Nara, T. Momma, T. Osaka, S. Shanmugam, *ACS Appl. Mater. Inter.* 6 (2014) 16545-16555.
38. Y. Li, M. Gong, Y. Liang, J. Feng, J.E. Kim, H. Wang, G. Hong, B. Zhang, H. Dai, *Nat. Commun.* 4 (2013) 1805.
39. L. Jörissen, *J. Power Sources* 155 (2006) 23-32.
40. Y. Liu, S. Chen, X. Quan, H. Yu, H. Zhao, Y. Zhang, G. Chen, *J. Phys. Chem. C* 117 (2013) 14992-14998.
41. K.N. Jung, J.H. Jung, W.B. Im, S. Yoon, K.H. Shin, J.W. Lee, *ACS Appl. Mater. Inter.* 5 (2013) 9902-9907.